Available online at www.sciencedirect.com
SCIENCE DIRECT
Thermochimica Acta 438 (2005) 35–40
thermochimica acta
www.elsevier.com/locate/tca

Comparative investigation of mortars from Roman Colosseum and cistern

D.A. Silva [a,*], H.R. Wenk [b], P.J.M. Monteiro [a]

[a] *Department of Civil and Environmental Engineering,725 Davis Hall 94720-1710, University of California at Berkeley, Berkeley, CA, USA*
[b] *Department of Earth and Planetary Science, 497 McCone 94720-4767, University of California at Berkeley, Berkeley, CA, USA*

Received 8 December 2004; received in revised form 28 February 2005; accepted 7 March 2005
Available online 9 September 2005

Abstract

Mortar from the Roman Colosseum and a Roman cistern from Albano Laziale were characterized with optical microscopy, scanning electron microscopy (SEM), X-ray diffraction (XRD), Fourier-transform infrared spectroscopy (FT-IR), and thermal analysis (differential scanning calorimetry (DSC) and thermogravimetric analysis (TGA)). The different techniques provided consistent results that the mortar of the Colosseum is mainly calcareous lime, while the mortar of the cistern is pozzolanic siliceous material. The study highlights the capabilities of the different methods for the analysis of cement. For routine analysis XRD is adequate but for characterization of poorly crystalline phases FT-IR and TGA have definite advantages.

Keywords: Ancient mortar; Roman Colosseum; Lime; Pozzolan; Microstructural characterization

1. Introduction

Lime has been used far back in antiquity as a cementitious material. Lime is a non-hydraulic cement and is dissolved by water. Over long periods it undergoes carbonation and converts to calcite. The Roman pozzolanic concrete relied on addition of tuffaceous volcanic material that was not widely available (the type locality is at Pozzuoli, near Naples) and Romans therefore used both lime and pozzolanic cement, depending on the application. Although the Romans were not the first to use reactive pozzolans to make concrete, they deserve credit for developing systematic application techniques [1–3].

This is evident from the Roman aqueducts, temples, and roads that exist even today and attest to the strength and durability of the Roman concrete. Malinowski [4] credits the construction methods as well as the high quality of well-compacted, nonshrinking concrete for excellent durability of the crack-free aqueduct linings. Knowledge about this material was lost in the Middle Ages. An intriguing question arose with an investigation of the Colosseum in Rome as to whether water resistant pozzolan cement was used or simply lime. This is significant in the context of verifying the claims of many scholars including Cassius Dio, chronicler of ancient Rome, that Emperor Titus filled the Colosseum with water and staged naval battles there.

To investigate the claim, we analyzed two samples of Roman cement. The first one is from the Colosseum that was constructed under Emperor Vespasian, inaugurated by Titus in 80 A.D. and completed by Domitian. The second one is from a cistern belonging to the Roman legion in Albano Laziale, about 30 km north of Rome and built in the 2nd century. We employed several techniques to characterize the mortars of the specimens and, in this comparative study, will emphasize FT-IR and DSC–TGA that have been proved

* Corresponding author at: UFSC/CTC/ECV, Caixa Postal 476, CEP 88040-900, Florianopolis, SC, Brazil. Tel.: +55 48 331 5176; fax: +55 48 331 5191.
E-mail address: denise@ecv.ufsc.br (D.A. Silva).

0040-6031/$ – see front matter © 2005 Elsevier B.V. All rights reserved.
doi:10.1016/j.tca.2005.03.003

to be useful techniques for investigating ancient mortars [5–7].

2. Materials and methods

Fragments of Colosseum and cistern concrete were first inspected with light microscopy and scanning electron microscopy. Also a 30 μm thin section was prepared for analysis with a petrographic microscope. Small fragments of the mortars were then fragmented with a mortar and pestle and particles of aggregate and binder were separated manually. The binder fragments were ground and sieved, and particles with diameter smaller than 40 μm were submitted to X-ray diffraction (XRD), Fourier-transform infrared spectroscopy (FT-IR), and thermal analysis (differential scanning calorimetry (DSC) and thermogravimetric analysis (TGA)).

The surface morphology of the samples was investigated with a LEO 430 SEM, using secondary electrons for imaging. The samples were carbon-coated and regions of interest were then analyzed for chemical composition with an energy-dispersive X-ray spectrometer (EDAX).

Thin sections of the samples were studied with a Nikon petrographic microscope in transmission, using crossed polarizers and images were recorded digitally.

XRD analyses were performed with a Rigaku X-ray diffractometer with Cu Kα radiation (λ = 1.54 Å), Cu filter on secondary optics, 45 kV power and 20 mA current. The powder sample was mounted on a quartz support to minimize background.

An ATI Mattson–Infinity Series FTIR^{TM} Fourier-transform infrared spectrometer was used, and the mortars were analyzed in KBr pellets. The spectra were traced in the range 4000–400 cm^{-1} (wave number), and the band intensities were expressed in transmittance (%). The infrared analysis permitted the identification of the main molecular groups present in the mortars.

The thermal analyses were performed in a simultaneous DSC–TGA equipment (TA Instruments, model SDT 2960). The experimental conditions were: (a) continuous heating from room temperature to 1000 °C at a heating rate of 10 °C/min; (b) N_2-gas dynamic atmosphere (85 cm^3 min^{-1}); (c) alumina, top-opened crucible; (d) sample mass: 15 mg approximately. DSC and TG curves were obtained. DTG curves were calculated in order to establish the onset and final temperatures of the reactions. The thermal analysis allowed the authors to obtain the following data: (i) reactions peak temperature and main effect (endothermic or exothermic); (ii) loss on ignition of the sample; (iii) content of bound water, which is the weight loss in the temperature range 200–600 °C; and (iv) content of CO_2 released during the decomposition of carbonate phases. All the weight losses are expressed as a function of the ignited weight of the sample, as suggested by Taylor [8].

3. Results and discussion

3.1. Petrographic microscope

The preliminary petrographic examination revealed striking differences between the two samples (Fig. 1). Both samples contained aggregate material with many volcanic constituents, easily recognizable by birefringence, interference colors and optic character. These constituents include plagioclase, pyroxene, and in the case of the cistern sample, large crystals of leucite such as the one shown in Fig. 1b. The difference lies in the mortar, filling the space between aggregate particles. In the case of the Colosseum sample, this space is almost uniquely filled by calcite, recognized by very bright colors (Fig. 1a), whereas the cistern sample has a mortar with

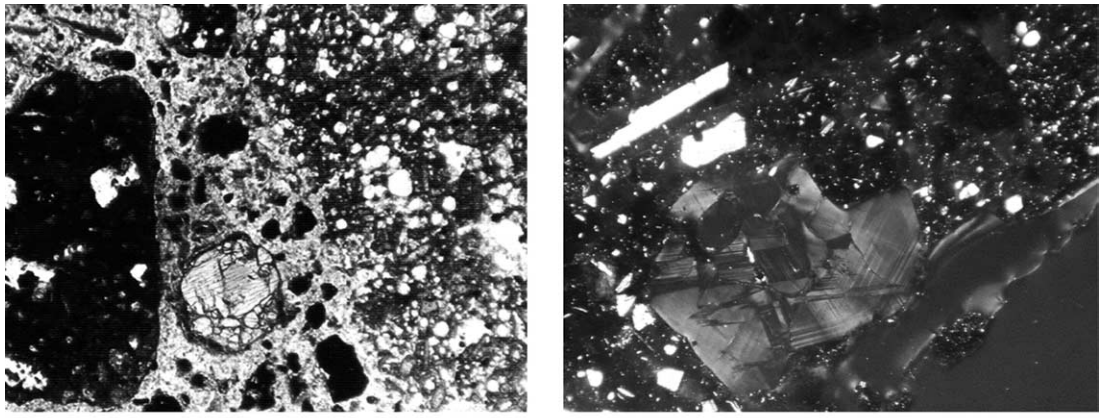

(a) Colosseum mortar (b) Cistern mortar

Fig. 1. Petrographic examination of thin sections of mortar from (a) Colosseum and (b) Albano cistern. Crossed polars. Both display fragments of volcanic crystals as aggregate, including a large leucite crystal with low colors and twinning (b). The Colosseum mortar is characterized by a matrix of highly birefringent calcite with bright colors (a).

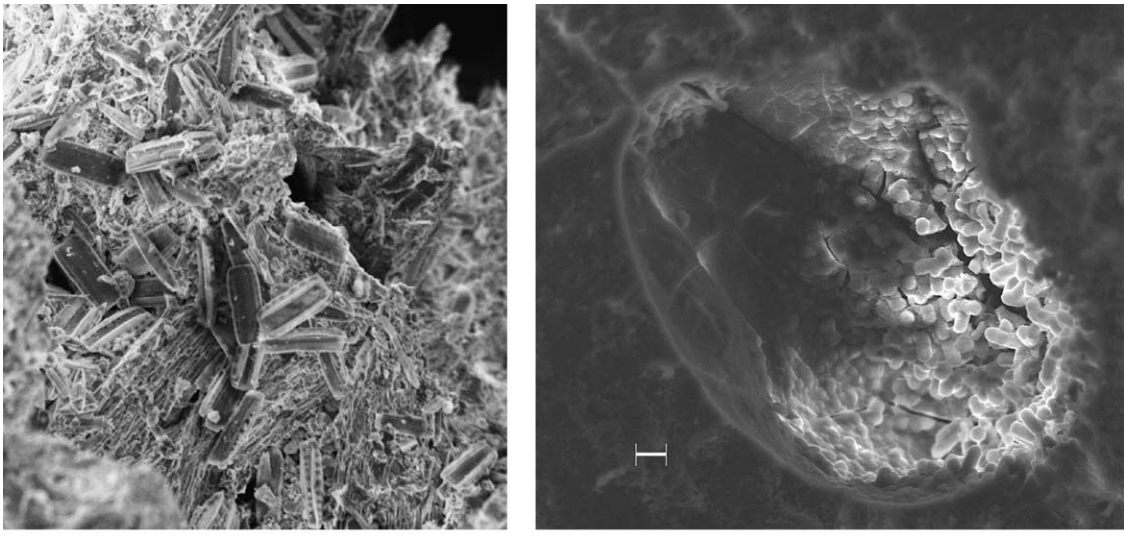

(a) Colosseum mortar (b) cistern mortar (scalebar is 30 μm)

Fig. 2. Secondary electrons SEM images of Colosseum mortar (a) and cistern mortar (b). The background of the Colosseum sample is an etched calcite crystal, covered with prismatic skeletons of diatoms. The cistern mortar is covered with a fine aggregation of highly siliceous material.

very low colors, consistent with poor crystallinity and amorphous character (Fig. 1b).

3.2. SEM

With the SEM it was easy to identify aggregate fragments such as mica, plagioclase and pyroxene, particularly with the help of EDAX. However, we focused the SEM investigation on small vugs in the matrix to reveal its composition and morphology. In the case of the Colosseum matrix, we observed large crystals of calcite with a slightly etched surface morphology. A chemical map only revealed Ca for these regions. Interestingly they are covered by small prismatic particles, 50–100 μm in length and a characteristic morphology with channels (Fig. 2a). They are composed of Si and we identify them as secondary skeletons of diatoms. Note that Malhotra and Mehta [9] classified diatoms as pozzolanic material, but in this case the skeletons are clearly secondary as shown by their perfect morphology and occurrence in cavities. The cistern matrix is composed of tiny aggregations and the compositional analysis reveals (in descending importance) Si, Al and Ca (Fig. 2b).

3.3. XRD

Both Colosseum and cistern mortars were analyzed under identical conditions and in both cases the sample was mounted on a quartz low background sample holder. Differences are striking. The Colosseum spectrum displays sharp diffractions that can all be attributed to calcite (Fig. 3). No other crystalline phases were detected. On the other hand, the spectrum obtained for the cistern mortar (Fig. 4) shows a broad diffuse peak in the range of 20°–40° (2θ), which is consistent with partially amorphous silicoaluminate hydrates.

3.4. FT-IR

Fig. 5 shows the infrared spectra of the Colosseum and cistern mortars. In the Colosseum mortar spectrum (Fig. 5a), the wave number bands at 2516 (over tone), 1799, 1421(ν_3), 875(ν_2) and 713 cm^{-1}(ν_4) are assigned to carbonate phases. On the other hand, the cistern mortar (Fig. 5b) only has traces of carbonates (slight bands at 1425, 1369 and 875 cm^{-1}). Both samples have strong bands related to the presence of bound water (around 3400 and 1630–1640 cm^{-1}). The water might be bound to hydraulic compounds, like silicate and aluminate hydrates.

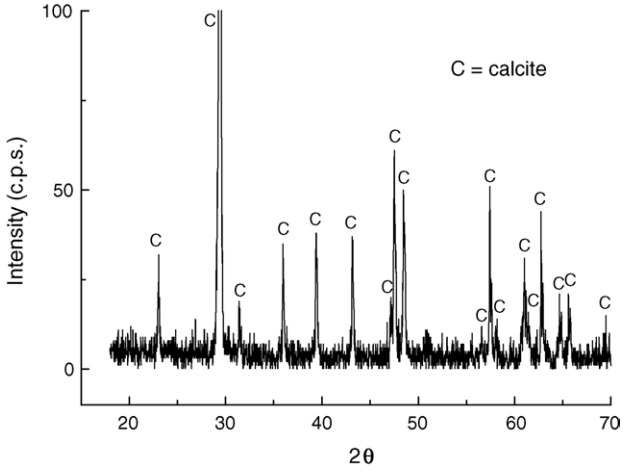

Fig. 3. XRD spectrum of Colosseum mortar with intense peaks of which most of them can be identified as calcite (c).

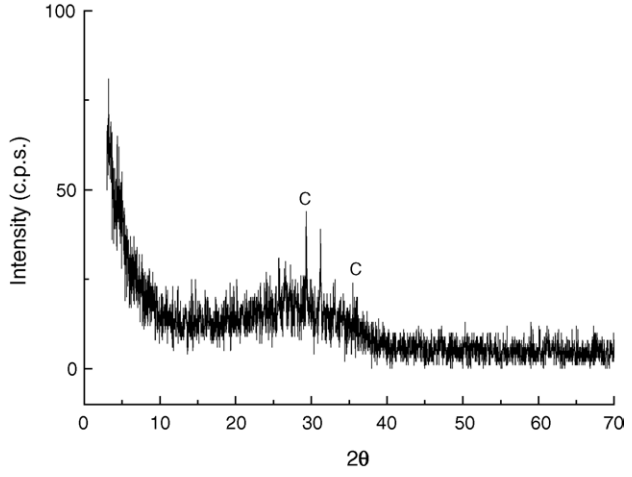

Fig. 4. XRD spectrum of the cistern mortar. The pattern shows no distinct diffraction peaks but only a diffuse maximum indicative of partially amorphous material. Conceivably a couple of peaks could be attributed to calcite (c).

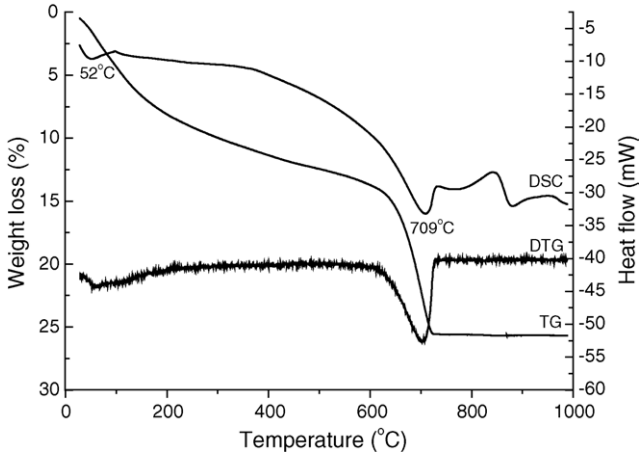

Fig. 6. DSC–TGA curves of Colosseum mortar.

Colosseum and cistern mortars present strong silicate bands (Si–O vibration) at 1035 and 1022 cm^{-1}, respectively. Silicate phases are also responsible for the bands at 463 and 451 cm^{-1} in Colosseum and cistern spectra, respectively. The silicate bands are stronger in the cistern than in the Colosseum sample, probably indicating a higher content of silicate phases in the cistern sample. The Al–O vibrations from silicoaluminate hydrates may also be responsible for the strong band at around 1000 cm^{-1} for both samples. If present, gypsum would produce bands at 1120 and 1145 cm^{-1} from S–O stretching vibrations [8]. However, due to the strong silicate bands in both samples, such bands can be obscured. Because a distortion of the silicate band towards higher wave lengths (around 1180 cm^{-1}) occurred in both spectra, the presence of gypsum in the mortars cannot be discarded from the infrared results. The gypsum could be originated from a voluntary addition during the mortars production or from the contamination of the mortars with polluted air or water [10]. In both Colosseum and cistern mortars there are two small peaks around 2920 and 2860 cm^{-1} that could be related to some organic material (stretching vibrations of the bond C–H in CH_2).

3.5. DSC–TGA

The simultaneously traced DSC–TG curves of both mortars are presented in Figs. 6 and 7. Two major endothermic reactions were identified during the heating of the Colosseum sample (Fig. 6): (a) release of the evaporable and adsorbed water at around 52 °C; (b) decomposition of the carbonate phases at around 709 °C, accompanied by a strong weight loss due to CO_2 release. After the first peak at 52 °C and up to around 600 °C, a quasi-constant weight loss rate is observed, and is mostly related to the dehydration of hydrated phases, such as silicates, aluminates or even clays.

In cistern sample (Fig. 7), two major reactions occurred during the heating: (a) release of free and adsorbed water (endothermic effect at around 120 °C) and (b) endothermic decomposition of carbonate phases at around 660 °C, which is associated with a weight loss of 2.26%. Furthermore,

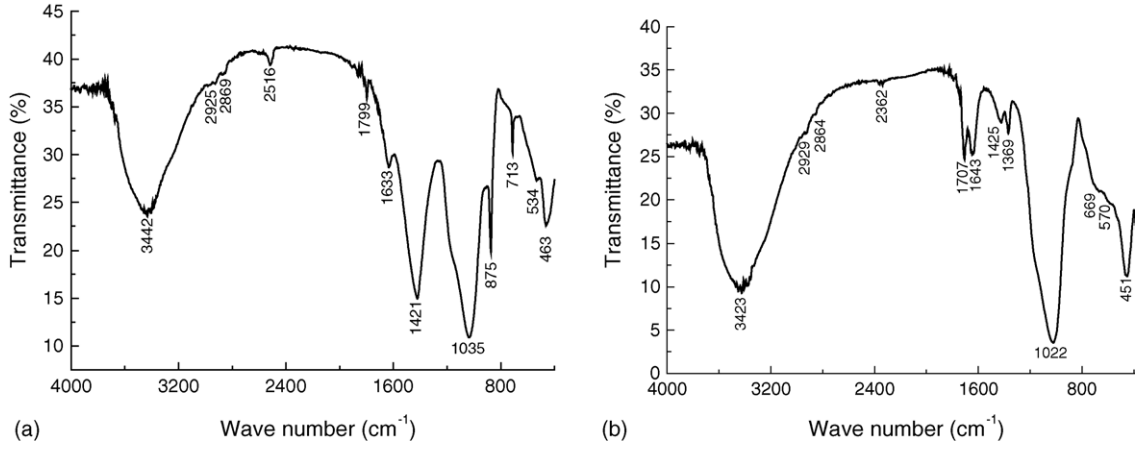

Fig. 5. Infrared spectra of (a) Colosseum and (b) cistern mortars.

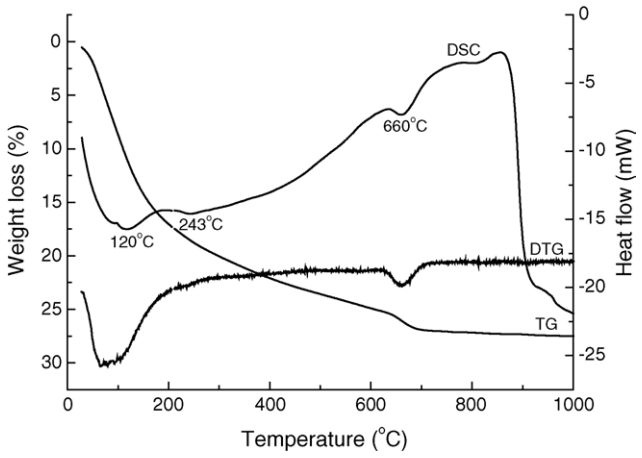

Fig. 7. DSC–TGA curves of cistern mortar.

there is a small peak in DSC and DTG curves at 243 °C, which could be related to the dehydration of silicoaluminate hydrates.

In agreement with the XRD and infrared results, the amount of carbonate phases measured by TG is much higher in Colosseum mortar than in cistern one. In the first mortar, the carbonate phases can be identified by the peak temperature at around 709 °C and the associated weight loss (11.88%), as shown in Fig. 6. Cistern mortar shows a peak at 660 °C attributed to decomposition of carbonates as well. The lower the decomposition temperature, the poorer crystallized is the carbonate. According to Paama et al. [11] and Moropoulou et al. [12], decomposition temperatures of calcium carbonate as low as 720 °C and less indicate that the carbonate is formed by recarbonation of lime, meaning that lime was added to both mortars as binder or plasticizer.

In order to evaluate how hydraulic the mortars are, the weight losses due to bound water release (200–600 °C) and to CO_2 release (600–800 °C) were determined. The first one can be due to the dehydration of calcium aluminate, calcium silicate or silicoaluminate hydrates originated from some pozzolanic reaction and the latter is due to the decomposition of carbonate phases, as already stated. According to Moropoulou et al. [12], the ratio CO_2/H_2O (hydraulic water) inversely represents the hydraulic character of a mortar in relation to CO_2 (weight loss, %). The results are shown in Tables 1 and 2 for the Colosseum and cistern mortars, respectively.

Table 1
Weight loss data of Colosseum sample

Reaction	Temperature range (°C)	Weight loss (%)
Whole analysis	25–1000	25.67
Release of adsorbed and part of bound water	25–200	8.10
Release of bound water	200–600	5.62
Release of CO_2	600–800	11.88
Ratio CO_2/H_2O	2.11	

Table 2
Weight loss data of cistern sample

Reaction	Temperature range (°C)	Weight loss (%)
Whole analysis	25–1000	27.42
Release of adsorbed and part of bound water	25–200	17.01
Release of bound water	200–600	7.84
Release of CO_2	600–800	2.25
Ratio CO_2/H_2O	0.287	

Moropoulou et al. [13] studied 50 samples of ancient mortars from the Byzantine and Ottoman periods, and plotted the graph shown in Fig. 8 correlating the ratio CO_2/H_2O with the mass of CO_2 released in the range 600–800 °C and classifying the mortars as *lime* (mixtures consisting mainly of calcite (∼80%) and quartz), *cementitious* (artificial conglomerate of gravel with sand, lime and volcanic earth as pozzolanic admixture) and *crushed brick* (mixtures of an exclusively calcitic, binding material with finely ground bricks). Since the weight loss related to CO_2 release is an indicative of the $Ca(OH)_2$ content of the original mortar, it is relatively easy to discriminate typical lime mortars from pozzolanic mortars. Colosseum and cistern results were also plotted in the graph. From this graph it would appear that both of them are mostly hydraulic. In order to corroborate the experimental technique we also analyzed a sample of travertine limestone, analogous to that used in Roman constructions (Fig. 9, Table 3). Besides the far location of the point in the graph (Fig. 8) due to the high amount of CO_2 released by the limestone sample under heating, the temperature of decomposition of the limestone (∼786 °C) is higher than the carbonate peak temperatures for Colosseum (∼709 °C) and cistern (∼660 °C) mortars, pointing out the nature of the carbonate formation, as mentioned earlier.

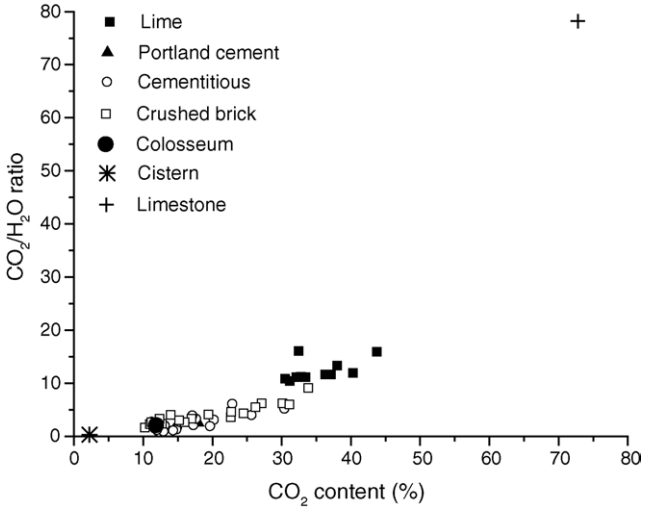

Fig. 8. CO_2/H_2O ratio × CO_2 content (% weight) for ancient mortars tested by Moropoulou et al. [13]. Data for Colosseum and cistern mortars and limestone are included.

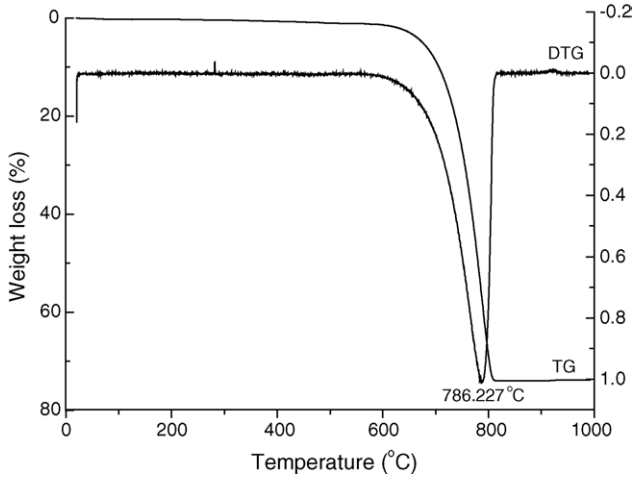

Fig. 9. TGA curves of pure limestone.

Table 3
Weight loss data of pure limestone

Reaction	Temperature range (°C)	Weight loss (%)
Whole analysis	25–1000	73.81
Release of adsorbed and part of bound water	25–200	0.27
Release of bound water	200–575	0.93
Release of CO_2	575–815	72.77
Ratio CO_2/H_2O	78.247	

None of the analyzed samples contains quartz, because the endothermic peak related to phase transformation of α to β quartz at around 570 °C was not detected.

4. Discussion and conclusions

Optical microscopy, SEM, XRD and FT-IR data are consistent with the conclusion that most of the Colosseum mortar is lime that has since then converted to calcite, whereas most of the cistern mortar is pozzolanic. Microscopy and XRD provide a quick characterization of the major constituents, while FT-IR in addition includes important information on minor and poorly crystalline components such as water content and silicoaluminate hydrates. The TGA analysis also suggests higher carbonate content for Colosseum than for cistern mortar, but the CO_2 percentage is still far below the theoretical number for pure calcite (78% of the final sample weight, which is the molar mass ratio CO_2/CaO). The reliability of the instrument was tested with limestone and this did indeed produce 73% (Table 3) which is near the theoretical value. It suggests that the Colosseum mortar used for the analysis did contain some silicate aggregate or did contain some amorphous silicoaluminate hydrates that were not detected with XRD which is not very sensitive for identifying amorphous phases, particularly in the presence of crystalline material. It highlights the complementary character of the different techniques: microscopy for a first assessment of morphology, XRD for identification of major crystalline phases, FT-IR for a more detailed assessment of composition that includes non-crystalline phases and TGA for a quantitative determination of volatile phases (particularly CO_2 and H_2O) that are characteristic for lime and pozzolanic mortars. In conclusion it appears that cistern mortar is a high quality pozzolanic material, consistent with the requirement of water resistance, whereas Colosseum mortar is a lower quality mortar with a different lime/pozzolan ratio, since requirements for water resistance were rather peripheral.

Acknowledgements

The authors acknowledge the financial support of CAPES (Fundação Coordenação de Aperfeiçoamento de Pessoal de Nível Superior, Ministério da Educação, Brasil). James Younger from Termite Productions provided samples and information. NSF supported this research. Suzanne Behrs, Tim Teague and Richard Brutchey assisted with some of the experiments that were conducted at the analytical facilities in the Chemistry and Earth Science Departments at the University of California at Berkeley.

References

[1] K.A. Harries, Concrete construction in early Rome, Concr. Int. (1995) 58–62.
[2] S.L. Marusin, Ancient concrete structures, Concr. Int. (1996) 56–58.
[3] E.G. Garrison, A History of Engineering and Technology: Artful Methods, CRC Press, 1991.
[4] R. Malinowski, Concrete and mortar in ancient aqueducts, Concr. Int. 1 (1979) 66–76.
[5] J. Adams, W. Kneller, D. Dollimore, Thermal analysis (TA) of lime- and gypsum-based medieval mortars, Thermochim. Acta 211 (1992) 93–106.
[6] S. Bruni, F. Cariati, P. Fermo, A. Pozzi, L. Toniolo, Characterization of ancient magnesian mortars coming from Northern Italy, Thermochim. Acta 321 (1998) 161–165.
[7] L. Paama, I. Pitkänen, P. Perämäki, Analysis of archaeological samples and local clays using ICP–AES, TG–DTG and FT-IR techniques, Talanta 51 (2000) 349–357.
[8] H.F.W. Taylor, Cement Chemistry, 2nd ed., Thomas Telford, London, 1997.
[9] V.M. Malhotra, P.K. Mehta, Pozzolanic and Cementitious Materials, Gordon & Breach, Amsterdam, 1996.
[10] C. Sabbioni, G. Zappia, C. Riontino, M.T. Blanco-Varela, J. Aguilera, F. Puertas, K. Van Balen, E.E. Toumbakari, Atmospheric deterioration of ancient and modern hydraulic mortars, Atmos. Environ. 35 (2001) 539–548.
[11] L. Paama, I. Pitkanen, H. Ronkkonmaki, P. Peramaki, Thermal and infrared spectroscopic characterization of historical mortars, Thermochim. Acta 320 (1998) 127–133.
[12] A. Moropoulou, A. Bakolas, K. Bisbikou, Characterization of ancient byzantine and later historic mortars by thermal and X-ray diffraction techniques, Thermochim. Acta 269/270 (1995) 779–795.
[13] A. Moropoulou, K. Polikreti, A. Bakolas, K. Bisbikou, P. Michailidis, Correlation of physicochemical and mechanical properties of historical mortars and classification by multivariate statistics, Cem. Concr. Res. 33 (2003) 891–898.